EUROFUSION WP14ER-PR(14) 12666

C Cazzaniga et al.

Response of LaBr3(Ce) scintillators to 14 MeV fusion neutrons

Preprint of Paper to be submitted for publication in
Nuclear Instruments and Methods in Physics Research
Section A

This work has been carried out within the framework of the EUROfusion Consortium and has received funding from the Euratom research and training programme 2014-2018 under grant agreement No 633053. The views and opinions expressed herein do not necessarily reflect those of the European Commission.

Response of $LaBr_3$(Ce) scintillators to 14 MeV fusion neutrons

C. Cazzaniga[1,2], M. Nocente[1,2], M. Tardocchi[2], M. Rebai[1], M. Pillon[3], F. Camera[4], A. Giaz[4], L.Pellegri[4] and G. Gorini[1,2]

[1]*University of Milano Bicocca, Departement of Physics, Piazza della Scienza 3, Milano 20125, Italy*
[2]*Istituto di Fisica del Plasma, Associazione EURATOM-ENEA-CNR, via Roberto Cozzi 53, Milano 20125 , Italy*
[3]*Associazione EURATOM-ENEA sulla Fusione ENEA C.R. Frascati, Via E. Fermi, 45, 00044 Frascati (Roma), Italy*
[4]*University of Milano, Departement of Physics, Via Celoria 16, Milano 1-20133 Italy*

carlo.cazzaniga@mib.infn.it

Keywords: Scintillators; Gamma-Ray Spectroscopy; Fast Neutrons; Burning Plasma

ABSTRACT
The response of a 3"x3" $LaBr_3$(Ce) scintillator to 14 MeV neutron irradiation has been measured at the Frascati Neutron Generator and simulated by means of a dedicated MCNP model. Several reactions are found to contribute to the measured response, with a key role played by neutron inelastic scattering and (n,2n) reactions on ^{79}Br, ^{81}Br and ^{139}La isotopes. An overall 43% efficiency to 14 MeV neutron detection above an experimental threshold of 0.35 MeV is calculated and confirmed by measurements. Post irradiation activation of the crystal has been also observed and is explained in terms of nuclear decays from the short lived ^{78}Br and ^{80}Br isotopes produced in (n,2n) reactions. The results presented in this paper are of relevance for the design of γ-ray detectors in burning plasma fusion experiments of the next generation, such as ITER, where capability to perform measurements in an intense 14 MeV neutron flux is required.

1. Introduction

Gamma-ray spectroscopy is among the diagnostics proposed to measure confined energetic ions in a high performance burning plasma, where the plasma behaviour is dominated by supra-thermal ions [1]. Energetic particles in the MeV range are naturally present in a burning deuterium-tritium plasma due to the main fusion reaction t(d,n)α and to auxiliary heating schemes. In a high power fusion device, γ-ray emission results from interactions between the energetic ions and impurities that are naturally found in the plasma [2-4]. Parameters of the fast ion energy distribution can be obtained by combining information on the intensity and shape of characteristic peaks of γ-ray reactions occurring in the plasma [5-7] as demonstrated with high energy resolution measurements in present tokamak devices [8-10].
Instrumentation for γ-ray spectroscopy measurements in a burning plasma (eg. ITER [11]) requires, in addition to good energy resolution, high count rate capabilities (>MHz).
$LaBr_3$(Ce) scintillators [12,14] are good candidates to meet these requirements, thanks to their fast scintillation time, high light yield and resilience to neutron damage. First measurements at low counting rates (kHz) at present tokamak devices have been recently performed [8,15]. Dedicated tests at nuclear accelerators demonstrated high counting rate performances up to 4 MHz without any significant degradation of the γ-ray energy resolution [7].
In a high power fusion device, besides coping with high counting rates, the detector will have to measure in a harsh environment at high neutron fluxes. A detailed study of the scintillator response to neutron irradiation is thus needed for the design of suitable line of sights, neutron filters and to aid in the measurement interpretation.
In a previous work, we presented the response of $LaBr_3$(Ce) scintillators to 2.5 MeV neutron irradiation [16], which is the dominant component in a deuterium plasma. Measurements were performed at the Frascati Neutron Generator (FNG) with 2.5 MeV mono-energetic neutrons and at tokamak devices run in deuterium. A dedicated MCNP model was used to interpret the results.
In this paper, we complete our previous investigation by presenting the response of $LaBr_3$(Ce) scintillators to 14 MeV neutron irradiation, which is most interesting for operations in deuterium-tritium plasmas. Measurements were carried out at FNG using a tritium doped target, rather than the deuterium doped target employed for 2.5 MeV neutron irradiation.
Similarly to our previous investigation, an MCNP model is used to aid in the interpretation of the results and, in particular, to identify the most relevant processes determining the measured response.

2. 14 MeV neutron measurements at FNG

At the Frascati Neutron Generator (FNG) 14 MeV neutron emission is obtained by reactions between a 300 keV deuterium beam impinging onto a tritium doped titanium target [17]. In our experiment, a 3"x3" (diameter x height) $LaBr_3$(Ce) scintillator was placed at 90 degrees with respect to the incoming deuterium beam, at the same height of the target. The circular face of the scintillator was facing the source. The distance from the target (1.25 m) was chosen so to obtain a neutron flux of about $2.4 \cdot 10^3$ n/(cm^2·s) on the detector front surface for a neutron yield of $5 \cdot 10^8$ n/s generated by the machine. The latter was measured by the standard neutron counting diagnostic of FNG, which consists of an absolutely calibrated detector measuring alpha particles produced by deuterium-tritium reactions in the

target. The impinging neutron energy spectrum at the detector position was centred at 14 MeV, with an estimated 1% (FWHM) energy spread.
The light emitted by the scintillator was collected by a photo-multiplier tube and signals were fed directly into a 12 bit - 250 Msample/s CAEN DT5720 digitizer. Each waveform above a selectable threshold was stored and processed off-line using a dedicated algorithm based on pulse fitting [7]. The pulse height spectrum was energy calibrated with laboratory ^{137}Cs and ^{60}Co radioactive sources. It is worth to point out that the step to neutron data (up to 14 MeV) requires a quite large extrapolation compared to the available calibration points. An energy resolution of 3.2% was measured at the 0.662 MeV line of ^{137}Cs, which is close to the nominal value expected for $LaBr_3$ crystals (about 3%). In the following, the letter E indicates the γ-ray (or electron equilavent) energy; a subscript is otherwise used to indicate the energy of a different particle.
Figure 1 shows the measured energy spectrum during 14 MeV neutron irradiation. Data were integrated over a time of 120 seconds. Gamma-rays peaks at distinctive energies and more complex structures can be clearly observed in the figure, with most of the events in the region E<3 MeV, where the detection efficiency to γ-rays is known to be higher [18]. There is however a clear tail of events extending to energies up to about E=14 MeV. An average count rate of $8 \cdot 10^4$ cps above the experimental E=0.35 MeV threshold was observed during measurements. After about 1 h of 14 MeV neutron irradiation, the FNG beam was switched off, and a post-irradiation measurement was started. Figure 1 shows the spectrum measured 10 minutes after irradiation, which can be compared to that obtained during irradiation, for the same experiment time. There is a clear difference in magnitude and shape between the two spectra. No events are found above E=4 MeV in the post-irradiation spectrum. Many of the structures observed during irradiation have also disappeared and the shape of the spectrum is now dictated by the superposition of beta decays of different short lived unstable isotopes (see section 5). An intense 511 keV annihilation peak still remains, together with a second peak at E=0.8 MeV. The post irradiation spectrum can also be compared to that due to the crystal intrinsic radioactivity (figure 1, dotted line). The latter was measured at FNG right before irradiation and also shows a 662 keV peak due to a ^{137}Cs calibration source. Again, we find no similarity between the two spectra, both in terms of structure and magnitude, which indicates that the post-irradiation spectrum must be dominated by decays of unstable isotopes generated by 14 MeV neutron irradiation. The contribution of intrinsic radioactivity to the count rate before neutron irradiation was 700 cps, a value much lower than the (average) $2.5 \cdot 10^4$ cps measured 10 minutes after neutron irradiation.

Figure 1: Energy spectrum measured at FNG with a 3''x3'' $LaBr_3$ detector during 14 MeV neutron irradiation (solid line). The spectrum is compared to that taken post (dashed) and before (dotted) irradiation. In all cases, measurements are integrated for 120 seconds.

3. Monte Carlo simulation of the $LaBr_3$ response

As discussed in our previous paper on 2.5 MeV neutrons [16], nuclear interactions between 14 MeV neutrons and lanthanum and bromine isotopes dominate the measured response. ^{79}Br and ^{81}Br are the Bromine isotopes in the crystal, with approximately the same abundance, while ^{139}La is the only stable isotope of Lanthanum. Few other isotopes are also present, but only in trace concentrations and were not considered in the analysis. Besides inelastic scattering, the

main neutron interaction mechanism with these isotopes is the production of secondary particles (neutrons, protons, deuterons, alpha particles) which in turn deposit their energy into the crystal, resulting in recordable pulses. The cross sections for the most relevant reactions are shown in figure 2. It is worth noticing here that there is a clear difference between the dominant neutron interaction channels with $LaBr_3$ at E_n=2.5 MeV and E_n=14 MeV: while at E_n=2.5 MeV inelastic scattering dominates the response [16], secondary particle production is the most important process at E_n > 10 MeV and, particularly, (n,2n) reactions. The latter have a multiplicative effect on the detector response: secondary neutrons generated in the crystal can in turn undergo nuclear inelastic scattering, which generates excited nuclear states decaying by γ-ray emission, that adds up to the detector gamma-ray load due to inelastic scattering of the primary (14 MeV) neutrons. Among the reactions leading to charge particle production, proton generation due to n+^{79}Br interactions is the most relevant.

A MCNP [19] model was implemented to interpret the experimental results, assuming a beam of mono-energetic 14 MeV neutrons directed onto a 3"x3" $LaBr_3$ and tracking all the processes listed in Figure 2. A summary of the results of this simulation is presented in Table 1, where numbers are normalized per 14 MeV neutron history. Of most interest is γ-ray production, that exceeds unity with 1.17 γ-rays produced per 14 MeV neutron. This result can be explained by the large additional contribution of secondary neutrons generated in the crystal (0.45), a fraction of which also undergoes inelastic scattering. Here we note that γ-rays born in the crystal volume have a significant detection probability (about 40%), given the large volume, high density and high Z of the scintillator, and are thus of relevance to understand the measured crystal response. Charged particle production is less important, mostly because of the smaller cross sections of the associated processes, although, on the other hand, positive ions have a detection probability approaching 100%. For comparison, the simulation was also run for a 3"x6" crystal, which is the size of the scintillator currently in use at JET [15]. As noted from Table 1, doubling the crystal volume determines a 55% increase in secondary neutron production, which is turn enhances gamma-ray creation by almost the same amount. Charged particle production remains small.

The contribution of secondary neutron/ gamma-rays and other particles to the crystal response was also analysed in terms of spectral shapes, as shown in Figure 3 for the 3"x3" case. γ-rays dominate in the region E < 5 MeV, while proton production contributes most to the spectral shape at E > 5 MeV, leading to a change of slope in this region. Alpha particle and deuterium generation introduces two additional structures centred around E=6 and E=10 MeV respectively, which are however an order of magnitude lower that that due to protons and would be hard to distinguish in the overall detector response, without using pulse shape discrimination algorithms as investigated in recent studies [20]. By summing up all the different contributions, we can determine a 43% detection efficiency to 14 MeV neutrons above the experimental threshold of 0.35 MeV, based on the MCNP results. The efficiency is defined as the number of counts above threshold per impinging neutron.

In order to compare the simulated response with that measured, a separated calculation of the (external) neutron/gamma-ray background in the FNG hall at the detector position was performed, which was finally added to the (intrinsic) response described above. In fact, the radiation field impinging on the detector in the FNG hall is a complex mixture of neutron and γ-rays. Of these two, the neutron field has a dominant 14 MeV (direct) component, with an additional scattering contribution at the 50% level, the latter arising from direct neutrons that degrade their energy by interacting with materials in the experimental hall. Gamma-ray background originates from inelastic scattering of the direct neutrons. For the calculation of the scattered neutron and gamma-ray fields, we relied on an existing MCNP model of the FNG facility [22]. Its results were in turn used as input to separately determine the crystal response to such background for comparison with measurement.

Table 2 summarizes the output of the calculations, with numbers normalized per 14 MeV neutron history. Scattered neutrons are responsible of about 50% of the detector load due to the primary component. Gamma-ray background contributes to a further 30% fraction. In terms of energy spectrum (Figure 4), the scattered neutron component has an exponential shape without clear structures, while gamma-rays are manifested as distinctive peaks and dominate the E > 4.5 MeV region. Figure 4 also shows the response to direct 14 MeV neutrons (presented in figure 3) and which can be here compared to background. In order to obtain the γ-ray equivalent energy for the direct component, quenching effects were taken into account [23-25]. The finite energy resolution of the detector was included in Figure 4 by convolution of the simulated spectra with a Gaussian function of energy dependent width. This was obtained from the measured value of 3.2% (FWHM/E) at 662 keV and assumed to follow the Poisson law, i.e. to scale as $E^{-½}$.

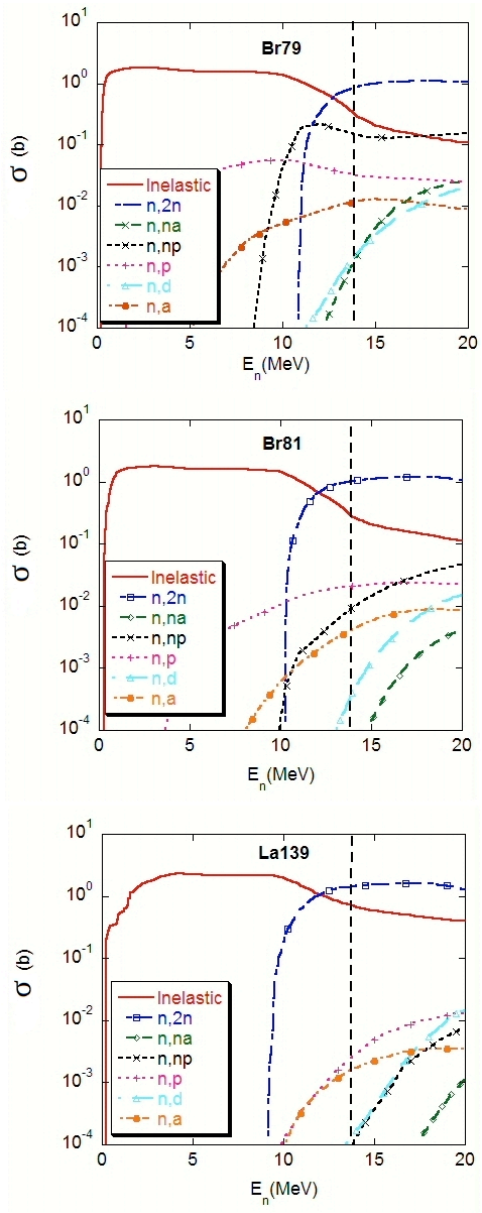

Figure 2: Cross sections for neutron reactions with ^{79}Br, ^{81}Br and ^{139}La isotopes leading to neutron, alpha particle, proton and deuteron production in the final states. The continuous line indicates the nuclear inelastic scattering cross section. The dashed vertical line is used to indicate E_n=14 MeV. Data taken from [20].

	$LaBr_3$ 3"x6"	$LaBr_3$ 3"x3"
gamma creation	1.868	1.178
neutron creation (n,2n)	$6.982 \cdot 10^{-1}$	$4.513 \cdot 10^{-1}$
proton creation	$1.53 \cdot 10^{-2}$	$9.54 \cdot 10^{-3}$
deuteron creation	$1.13 \cdot 10^{-3}$	$7.63 \cdot 10^{-4}$
alpha creation	$1.58 \cdot 10^{-3}$	$1.10 \cdot 10^{-3}$

Table 1: Results of MCNP simulations of the $LaBr_3$ response to 14 MeV neutrons regarding production of secondary particles of different types (γ, n, p, d, a). Simulations were performed for two different crystal dimensions (3"x3" and 3"x6"). Results are normalized per 14 MeV neutron history.

Figure 3: Deposited energy spectrum from secondary particles produced by uniform irradiation of a 3"x3" LaBr3 crystal with 14 MeV neutrons, as calculated by MCNP.

Counts from direct 14 MeV neutrons	0.432
Counts from scattered neutrons at FNG	0.206
Counts from gamma background at FNG	0.138
Sum	0.776

Table 2: Summary of MCNP simulations of primary and background radiation (above a threshold of 350 keVee) recorded by $LaBr_3$ in the 14 MeV irradiation experiment at FNG, at the detector position. Results are normalized per 14 MeV neutron history.

Figure 4: Simulated pulse height spectra from direct 14 MeV neutrons, scattered neutrons and gamma-ray background recorded at the detector position in the FNG irradiation experiment. Energies are electron equivalent and take into account quenching effect.

4. Data analysis

The results of the MCNP simulations are compared to the measured spectrum in Fig. 5. To this extent, the three components of Figure 4 (direct and scattered neutrons, gamma-ray background) were summed to obtain the expected measured spectrum during the FNG irradiation experiment. The comparison is limited to 3 orders of magnitude below the most intense spectral structures, a range that well exceeds the accuracy needs for the use of $LaBr_3$ in gamma-ray spectroscopy applications at ITER. In terms of count rates above the 0.35 MeV experimental threshold, we find that measurement and simulation agree within 5%. A similar good level of agreement also holds as far as the overall shape of the spectrum is concerned. In particular, when shown in logarithmic scale, the measured spectrum exhibits the change of slope predicted by MCNP in the region 5 - 10 MeV and due to the contribution of secondary charged particles (see section 3). At a more detailed level, we find that most of the gamma-ray peaks observed in the measurement are also reproduced by the simulation, although, at times, there is a mismatch in terms of intensity. In few cases only, peaks predicted in the simulation do not appear in the measurement, and vice versa. We ascribe these minor differences to uncertainties in the cross sections used by MCNP, especially since they are derived by statistical models, which may not accurately depict reality [26]. A second source of uncertainty arises from the FNG model, which may not specify the material composition of the experimental hall at a level of detailed necessary to explain all peaks found in the measurement. In spite of these minor discrepancies, we consider the level of agreement between simulation and measurement as satisfactory, given the capability of the simulation to match well the experimental count rate and spectral shape, which are of most interest to design filters for neutron background reduction on the scintillator at ITER [11]. In this context, we note in particular that the measured spectrum is rather structureless in the range E=3 to 5 MeV, i.e. where gamma-ray lines from plasma reactions of principal interest in thermonuclear fusion applications occur.

Figure 5: Measured and simulated energy spectrum (linear and log scale) of the $LaBr_3$ response to 14 MeV neutrons at FNG. The two panels have different energy scale in order to emphasise different parts of the spectrum. The simulated spectrum is the sum of the three components (direct and scattered neutrons, gamma-ray background) shown separately in Figure 4. The direct component also includes events from secondary charged particles, as discussed with reference to Figure 3.

5. Short lived activation induced by 14 MeV neutrons

Activation of the $LaBr_3$ crystal is of interest in view of ITER for two reasons. First, a significant activation level requires some special care when handling the crystal after an extended irradiation period. Secondly, the activation itself is a background source that interferes with the measured signal and is thus of relevance for signal-to-noise ratio considerations in view of measurements at ITER. In order to investigate the activation of the crystal induced by 14 MeV neutrons, post-irradiation measurements were carried out at FNG. The $LaBr_3$ crystal was first irradiated for about 1.5 h at a total neutron yield of $1.5 \cdot 10^{10}$ neutrons per second, corresponding to a flux on the detector front surface of approximately $5.4 \cdot 10^5$ neutrons/(s·cm^2). A measurement of the residual count rate, as a function of time, due to the crystal activation was then started immediately after FNG had been switched off, with the results shown in Figure 6. Data points were acquired every second, for 30 minutes.

Based on our previous analysis [16], short lived activation is expected to be due to ^{78}Br and ^{80}Br isotopes, which have a decay time of 540 s and 1500 s, respectively. ^{78}Br and ^{80}Br are produced by (n,2n) reactions on ^{79}Br and ^{81}Br. On the other hand, the (n,2n) reaction on ^{139}La produces ^{138}La, which has a half life of billions of years, and is therefore

practically stable on the time scale of minutes.
The conclusions of our previous analysis are experimentally confirmed by a fit to the measurement of Figure 6 using the following equation

$$I = A \cdot exp\left(-\frac{t}{\tau_1}\right) + B \cdot exp\left(-\frac{t}{\tau_2}\right) + C \qquad (1)$$

where I indicates the intensity (count rate) and t is the time. In equation 1 the time constants τ_1 and τ_2 were fixed and set to the decay times of ^{78}Br (540 s) and ^{80}Br (1500 s). The free fit parameters A, B are proportional to the initial number of ^{78}Br and ^{80}Br nuclei produced by 14 MeV irradiation. C is a fit parameter that takes into account long lived (τ >> 30 min) activation, such as that due to materials of the FNG hall that were also activated by 14 MeV neutrons. As seen from Figure 6, the fit reproduces very well the measurements, confirming the role of ^{78}Br and ^{80}Br as main responsible of the crystal post-irradiation activity. The values obtained for the fit parameters A,B and C are summarized in Table 3.

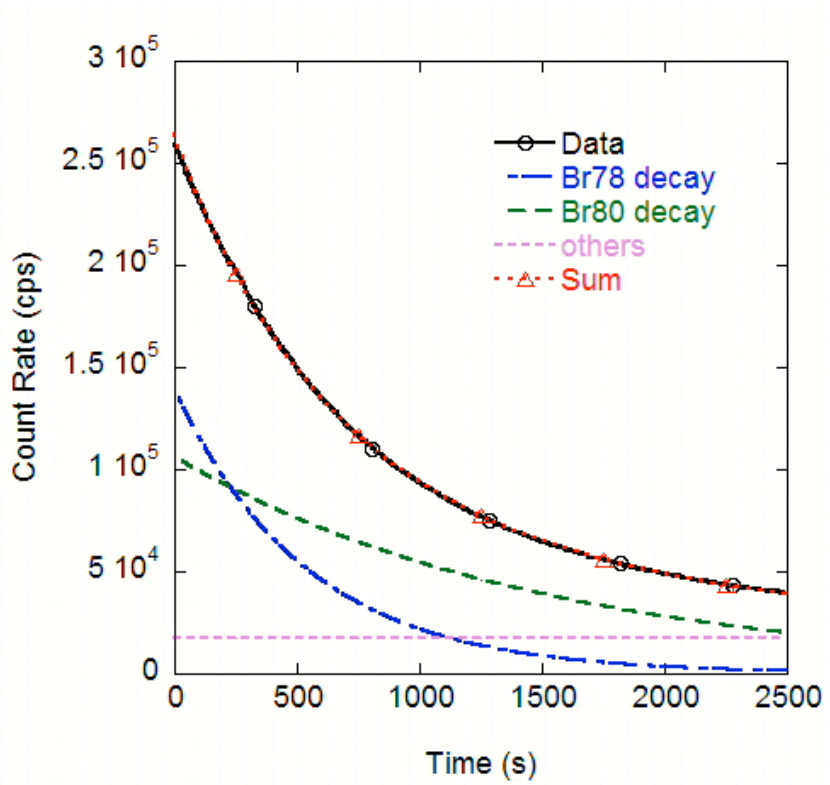

Figure 6: $LaBr_3$ count rate as a function of time measured after 1.5 h of 14 MeV neutron irradiation at FNG. The measurement was started immediately after the machine switch off. A fit with eq. 1 is also shown (dashed line with symbols), together with individual curves for the three sources (^{78}Br, ^{80}Br and others) contributing to the measured activation (see text for details).

Fit Parameter	Value (cps)	Error (cps)
A	$1.279 \cdot 10^5$	$\pm 1.6 \cdot 10^2$
B	$1.005 \cdot 10^5$	$\pm 1.6 \cdot 10^2$
C	$1.794 \cdot 10^4$	$\pm 5 \cdot 10^1$

Table 3. Values of the fit parameters A,B and C as obtained by fitting data in Figure 6 with Eq. 1

6. Conclusions

The response of a 3"x3" $LaBr_3$ crystal to 14 MeV neutron irradiation was measured at FNG in a dedicated experiment. The results were interpreted by means of a MCNP model of 14 MeV neutron interactions with $LaBr_3$, including background contributions from scattered neutrons and gamma-rays generated in the FNG experimental hall. A good overall agreement between simulation and measurements was found. These measurements are novel with respect to the previously
reported response function at 2.5 MeV, since the interaction physics of 14 MeV neutrons with the
crystal is completely different. The simulations revealed that (n,2n) reactions and nuclear inelastic scattering on ^{79}Br, ^{81}Br and ^{139}La isotopes are the dominant interaction processes of 14 MeV neutrons in the crystal. Reactions leading to the production of secondary charged particles are of relevance to explain events at deposited energies higher than 5 MeV. The overall efficiency of the 3"x3" detector to 14 MeV neutrons was found to be 43%, above an experimental threshold of 0.35 MeV. Measurements of the residual crystal activation after irradiation were also performed and were found to be dominated by decays of short lived ^{78}Br and ^{80}Br isotopes produced by (n,2n) reactions. The results presented in this paper are of relevance for the design of γ-ray detectors in burning plasma fusion experiments of the next generation, such as ITER, where capability to perform measurements in an intense 14 MeV neutron flux is required.

Acknowledgement

This work has been carried out within the framework of the EUROfusion Consortium and has received funding from the European Union's Horizon 2020 research and innovation programme under grant agreement number 633053. The views and opinions expressed herein do not necessarily reflect those of the European Commission.

References

[1] Fasoli, A., C. Gormenzano, H. L. Berk, B. Breizman, S. Briguglio, D. S. Darrow, N. Gorelenkov et al. "Physics of energetic ions." *Nuclear Fusion* 47, no. 6 (2007): S264.

[2] Kiptily, V. G., F. E. Cecil, and S. S. Medley. "Gamma ray diagnostics of high temperature magnetically confined fusion plasmas." *Plasma physics and controlled fusion* 48, no. 8 (2006): R59.

[3] Tardocchi, M., M. Nocente, and G. Gorini. "Diagnosis of physical parameters of fast particles in high power fusion plasmas with high resolution neutron and gamma-ray spectroscopy." *Plasma Physics and Controlled Fusion* 55.7 (2013): 074014.

[4] Kiptily, V. G., F. E. Cecil, O. N. Jarvis, M. J. Mantsinen, S. E. Sharapov, L. Bertalot, S. Conroy et al. "γ-ray diagnostics of energetic ions in JET." *Nuclear Fusion* 42, no. 8 (2002): 999.

[5] Cecil, F. E., and David E. Newman. "Diagnostics of high temperature deuterium and tritium plasmas by spectrometry of radiative capture reactions." *Nuclear Instruments and Methods in Physics Research* 221, no. 2 (1984): 449-452.

[6] Proverbio, I., M. Nocente, V. G. Kiptily, M. Tardocchi, G. Gorini, and JET-EFDA Contributors. "The ^{12}C (^{3}He, pγ) ^{14}N reaction cross section for γ-ray spectroscopy simulation of fusion plasmas." *Review of scientific instruments* 81, no. 10 (2010): 10D320-10D320.

[7] Nocente, M., M. Tardocchi, A. Olariu, S. Olariu, R. C. Pereira, I. N. Chugunov, A. Fernandes et al. "High Resolution Gamma Ray Spectroscopy at MHz Counting Rates With LaBr Scintillators for Fusion Plasma Applications." *Nuclear Science, IEEE Transactions on* 60, no. 2 (2013): 1408-1415.

[8] Nocente, M., M. Garcia-Munoz, G. Gorini, M. Tardocchi, A. Weller, S. Akaslompolo, R. Bilato et al. "Gamma-ray spectroscopy measurements of confined fast ions on ASDEX Upgrade." *Nuclear Fusion* 52, no. 9 (2012): 094021.

[9] Tardocchi, Marco, M. Nocente, I. Proverbio, V. G. Kiptily, P. Blanchard, Sean Conroy, M. Fontanesi et al. "Spectral Broadening of Characteristic γ-Ray Emission Peaks from ^{12}C (^{3}He, pγ)^{14} N Reactions in Fusion Plasmas." *Physical review letters* 107, no. 20 (2011): 205002.

[10] Nocente, Massimo, Marco Tardocchi, V. G. Kiptily, Patrick Blanchard, I. Chugunov, Sean Conroy, T. Edlington et al. "High-resolution gamma ray spectroscopy measurements of the fast ion energy distribution in JET 4He plasmas." *Nuclear Fusion* 52, no. 6 (2012): 063009.

[11] I.N. Chugunov, A.E. Shevelev, D.B. Gin, V.G. Kiptily, G. Gorni, M. Nocente, M. Tardocchi, D.N. Doinikov, V.O. Naidenov and E.M. Khilkevitch " Development of gamma-ray diagnostics for ITER", *Nucl. Fusion* 51 (2011) 083010

[12] Van Loef, E. V. D., P. Dorenbos, C. W. E. Van Eijk, K. W. Krämer, and H. U. Güdel. "Scintillation properties of $LaBr_3:Ce^{3+}$ crystals: fast, efficient and high-energy-resolution scintillators." *Nuclear Instruments and Methods in Physics Research Section A: Accelerators, Spectrometers, Detectors and Associated Equipment* 486, no. 1 (2002): 254-258.

[13] Nicolini, R., F. Camera, N. Blasi, S. Brambilla, R. Bassini, C. Boiano, A. Bracco et al. "Investigation of the properties of a 1 ″× 1 ″ $LaBr_3$:Ce scintillator." *Nuclear Instruments and Methods in Physics Research Section A: Accelerators, Spectrometers, Detectors and Associated Equipment* 582, no. 2 (2007): 554-561.

[14] Giaz, A., Pellegri, L., Riboldi, S., Camera, F., Blasi, N., Boiano, C., ... & Wieland, O. (2013). Characterization of large volume 3.5 ″× 8 ″$LaBr_3$: Ce detectors. *Nuclear Instruments and Methods in Physics Research Section A: Accelerators, Spectrometers, Detectors and Associated Equipment*, *729*, 910-921.

[15] Nocente, M., M. Tardocchi, I. Chugunov, R. C. Pereira, T. Edlington, A. M. Fernandes, D. Gin et al. "Energy resolution of gamma-ray spectroscopy of JET plasmas with a LaBr scintillator detector and digital data acquisition." *Review of scientific instruments* 81 (2010): 10D321.

[16] Cazzaniga, C., Nocente, M., Tardocchi, M., Croci, G., Giacomelli, L., Angelone, M., ... & Contributors, J. E. (2013). Response of $LaBr_3$ (Ce) scintillators to 2.5 MeV fusion neutrons. *Review of Scientific Instruments*, *84*(12), 123505.

[17] Martone, M., M. Angelone, and M. Pillon. "The 14 MeV frascati neutron generator." *Journal of nuclear materials* 212 (1994): 1661-1664.

[18] Cazzaniga, C., Croci, G., Giacomelli, L., Grosso, G., Nocente, M., Tardocchi, M., ... & Weller, A. (2013). $LaBr_3$ scintillator response to admixed neutron and γ-ray fluxes. *Nuclear Instruments and Methods in Physics Research Section A: Accelerators, Spectrometers, Detectors and Associated Equipment*, *732*, 384-387.

[19] The MCNPX website: http://mcnpx.lanl.gov/

[20] Cross Section Database http://atom.kaeri.re.kr/

[21] Crespi, F. C. L., Camera, F., Blasi, N., Bracco, A., Brambilla, S., Million, B., ... & Owens, A. (2009). Alpha–gamma discrimination by pulse shape in $LaBr_3$: Ce and $LaCl_3$: Ce. *Nuclear Instruments and Methods in Physics Research Section A: Accelerators, Spectrometers, Detectors and Associated Equipment*, *602*(2), 520-524.

[22] Angelone, M., Pillon, M., Batistoni, P., Martini, M., Martone, M., & Rado, V. (1996). Absolute experimental and numerical calibration of the 14 MeV neutron source at the Frascati neutron generator. *Review of scientific instruments*, *67*(6), 2189-2196.

[23] Cazzaniga, C., Nocente, M., Tardocchi, M., Fazzi, A., Hjalmarsson, A., Rigamonti, D., ... & Gorini, G. (2014). Thin YAP: Ce and $LaBr_3$: Ce scintillators as proton detectors of a thin-film proton recoil neutron spectrometer for fusion and spallation sources applications. *Nuclear Instruments and Methods in Physics Research Section A: Accelerators, Spectrometers, Detectors and Associated Equipment*, *751*, 19-22.

[24] Fazzi, A., Nocente, M., Tardocchi, M., Varoli, V., Gorini, G., Lorenzoli, M., ... & Cazzaniga, C. (2013, October). A large area SiPM array coupled to a $LaBr_3$ crystal for a TPR spectrometer. In *Nuclear Science Symposium and Medical Imaging Conference (NSS/MIC), 2013 IEEE* (pp. 1-4). IEEE.

[25] M. Nocente, A. Fazzi, M. Tardocchi, C. Cazzaniga, M. Lorenzoli, C. Pirovano, M. Rebai, C. Uboldi, V. Varoli and G. Gorini, "Experimental investigation of silicon photomultipliers as compact light readout systems for gamma-ray spectroscopy applications in fusion plasmas", *Rev. Sci. Instrum*. 85 (2014) 11E108

[26] A.J. Koning, S. Hilaire, M.C. Duijvestijn, □http://www.talys.eu/tendl-2008/□